MABS
2020, VOL. 12, NO. 1, 11
https://doi.org/10.1080/19420862.2020.1832861

Taylor & Francis
Taylor & Francis Group

REPORT

OPEN ACCESS Check for updates

Cross-species/cross-modality physiologically based pharmacokinetics for biologics: 89Zr-labelled albumin-binding domain antibody GSK3128349 in humans

Armin Sepp[a], Mats Bergström[b], and Marie Davies[c]

[a]IVIVT Modeling and Simulation, GlaxoSmithKline Plc, Stevenage, UK; [b]Cell Therapy RU, GlaxoSmithKline Plc, Stevenage, UK; [c]Research CPEM, GlaxoSmithKline Plc, Stevenage, UK

ABSTRACT

Two-pore physiologically-based pharmacokinetics (PBPK) for biologics describes the tissue distribution and elimination kinetics of soluble proteins as a function of their hydrodynamic radius and the physiological properties of the organs. Whilst many studies have been performed in rodents to parameterize the PBPK framework in terms of organ-specific lymph flow rates, similar validation in humans has been limited. This is mainly due to the paucity of the tissue distribution time course data for biologics that is not distorted by target-related binding. Here, we demonstrate that a PBPK model based on rodent data provided good to satisfactory extrapolation to the tissue distribution time course of ^{89}Zr-labeled albumin-binding domain antibody (AlbudAb™) GSK3128349 in healthy human volunteers, including correct prediction of albumin-like plasma half-life, volume of distribution, and extravasation half-life. The AlbudAb™ used only binds albumin, and hence it also provides information about the tissue distribution kinetics and turnover of that ubiquitous and multifunctional plasma protein.

ARTICLE HISTORY
Received 15 April 2020
Revised 23 September 2020
Accepted 1 October 2020

KEYWORDS
Human; domain antibody; AlbudAb™; albumin; antibody; immunoPET; physiologically based pharmacokinetics; PBPK; ibalizumab

Introduction

An increasing number of diverse novel biologic modalities are making their way toward the clinic,[1, 2] including domain antibodies (dAbs),[3,4] Nanobodies®,[5] bispecific T-cell engagers,[6] engineered scaffolds from fibronectin,[7] ankyrin repeat[8] or lipocalin,[9] and those that combine evolutionarily distant protein domains into a single molecule, like ImmTACs, which combine T cell receptors with single-chain variable fragments.[10] It is therefore desirable to have a quantitative framework for predicting the tissue distribution properties of these and any other biologic modalities along the guidelines of Three Pillars Paradigm[11] so that informed decisions can be taken for dosing and affinity requirements.

Physiologically based pharmacokinetics (PBPK) provide a quantitative mechanistic framework for describing the absorption, distribution, metabolism and excretion (ADME) of drugs in the species of interest. In the case of proteins, the most flexible approach is often described in terms of two-pore hypothesis proposed by Rippe and Haraldsson[12] where extravasation is linked to the lymph flow and treated as a filtration-diffusion process taking place at the paracellular vascular pores. Previously we showed in theory and practice that the filtration and diffusion-driven fluxes can be treated as linear functions of the lymph flow rate in such systems,[13] and followed up with an extensive study in mice and rats where the same framework was applied to a number of different biologics to estimate the organ-specific fractional lymph flow rates as the only empirically fitted global parameters.[14]

Here, we evaluate the rodent data-based biologics PBPK model by comparing its predictions for humans with the experimental observations from a recent Phase 1 clinical study (NCT02829307) where the tissue distribution time course of ^{89}Zr-labeled albumin-binding domain antibody (AlbudAb™) GSK3128349 was measured by positron emission tomography-computed tomography (PET/CT) in healthy volunteers.[15] In addition, we demonstrate how the resulting cross-species/cross-modality two-pore biologics PBPK framework can be adapted to a clinically relevant scenario for therapeutically relevant insight.

Results

Human biologics PBPK model calibration

AlbudAb-albumin interaction is analyzed according to the reaction scheme outlined on Figure 1, where the complex is in reversible equilibrium with the free species and the ^{89}Zr label can be irreversibly lost from the chelate. These reactions are coded into a PBPK model shown on Figure 2(a) which includes all major organs, with model-specific parameters listed in Table 1. Each organ contains the vascular, interstitial, and endosomal compartments, as outlined on Figure 2(b), while the brain and kidneys are further modified to describe the flow of interstitial fluid and renal filtration respectively.

The default PBPK parameters predicted 13.5 day half-life and 25% renal elimination for albumin in humans, which were shorter and higher relative to the respective experimental observations of 17–19 days[23,24] and 3–10%.[25,26] Both deviations indicated that the albumin glomerular sieving coefficient 0.0006, as calculated from the 67 kDa molecular weight using an empirical formula described by us before,[14] whilst in

CONTACT Armin Sepp armin.z.sepp@gsk.com Glaxo Medicines Research CentreGlaxoSmithKline Plc, Stevenage SG1 2NY, UK
Supplemental data for this article can be accessed on the publisher's website.

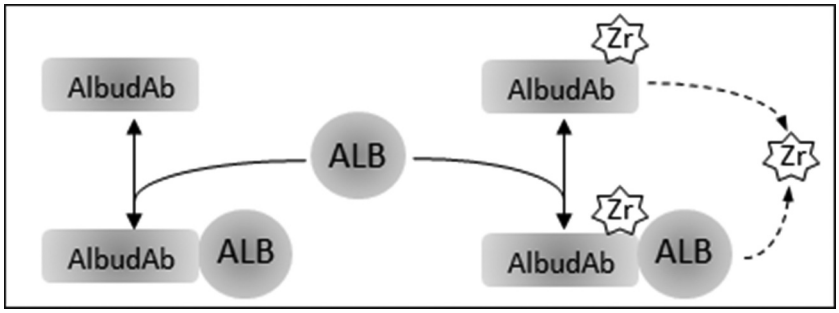

Figure 1. Interactions modeled for AlbudAb GSK3128349 PBPK. ALB: endogenous albumin at constant concentration. AlbudAb in unlabeled or ^{89}Zr-complexed format. Zr denotes both free label as well as ^{89}Zr-AlbudAb which has lost affinity for albumin. Solid arrows denote reversible binding of AlbudAb to albumin. Dashed arrow is a combined reaction which denotes irreversible loss of ^{89}Zr from the chelate or inactivation of the AlbudAb. Detailed reaction scheme for all molecular species and which includes vascular, interstitial, and endosomal compartments is shown on Supplementary Figure 1.

agreement with mouse and rat data,[27] was too high for humans. Five-fold adjustment of the glomerular sieving coefficient for free albumin and all albumin-containing complexes to approximately 0.00008, as estimated by Norden et al.[28] for humans, increased the terminal half-life to 17.5 days (Supplementary Figure 3) and reduced the fraction of renally eliminated albumin to 6%, both within physiological range. The adjusted values were thereafter stored in variant 'albumin' and used for all subsequent work.

The PBPK model-predicted steady state average interstitial fluid concentration of albumin in different tissues was 275 ± 118 μM (i.e., around 50% of plasma, close to the experimentally estimated value of 40%[29]), with median 278 μM, the highest 444 μM (liver) and the lowest 0.1 μM (brain)). The steady-state free interstitial endogenous albumin concentrations and those of endosomal complex with the neonatal Fc receptor (FcRn) were stored in SimBiology model variant 'end alb STST' and used as initial conditions in all subsequent calculations.

Kidneys and brain

The initial evaluation of the plasma PK calibrated AlbudAb model predictions against the ^{89}Zr-GSK3128349 AlbudAb tissue distribution data[15] revealed higher than expected PET signal in the kidneys, while the opposite was found for the brain. Given that ^{89}Zr is a residualizing radioisotope, unlike ^{3}H that we used previously in rodents,[14] the model was manually modified, as outlined in the Supplementary section, to evaluate the possible effect of a small fraction of inactive ^{89}Zr-labeled AlbudAb, or free ^{89}Zr present in the dose or leaking from the desferrioxamine (DFO) chelator, that may have contributed to the residualized ^{89}Zr in kidneys and brain. The tissue concentration time profiles were used to run SimBiology global nonlinear least squares fitting task 'Fit8 Data_org_all' to estimate the respective parameters, as presented in Table 2. The fitted tissue concentration data and predictions for capillary plasma and interstitial concentrations are shown on Figure 3(a) for the kidneys and Figure 3(b) for the brain.

The model-fitted adjustments describe the rapid initial accumulation of a small amount of ^{89}Zr in the kidneys, followed by slow clearance. In the case of the brain, the fitted model suggests very low concentration of ^{89}Zr-containing species in the interstitial space, effectively confining the entire brain signal to the vasculature only. There is no indication of detectable contribution from extravasation or accumulation even from macropinocytosis, in the timeframe studied.

Plasma

The calibrated PBPK model predicts biphasic plasma time course of ^{89}Zr-GSK3128349 AlbudAb with the distribution phase lasting around 4 days and the terminal half-life $t_{½}$ ≈18 days. The latter value is identical to that of human albumin, indicating that most of the AlbudAb exists in tight and stable complex with that ubiquitous plasma protein. The impact of adjusted brain- and kidney-related parameters on the plasma concentration profile is negligible, as shown on Figure 4.

The rest of the organs

Both the default and adjusted PBPK model variants were analyzed for the remaining organs for which data was available, as shown on Figure 5(a-f) for muscle, lungs, liver, bone marrow, pancreas, and spleen respectively. In the organs analyzed, the steady-state tissue concentrations reach the model-predicted levels, and, in most cases, this also extends to the distribution phase that is most characteristic of the tissue permeability properties.

In skeletal muscle (Figure 5(a)), the defining characteristic of the distribution phase is increasing total tissue concentration of ^{89}Zr-GSK3128349 AlbudAb at the time when its plasma concentration is declining. This can be understood in terms of relatively slow extravasation into a relatively large interstitial space before steady state is established, but a cellular clearance cannot be excluded.

In contrast, in the lungs and liver (Figure 5(b,c)) the plasma and tissue concentration time courses run in parallel from the beginning. Both these organs are highly vascularized with relatively large capillary and moderate interstitial volume. Furthermore, in the lung, tissue is characterized by higher hydrodynamic conductance assigned to the large pore fraction, while in the liver this is further amplified by the apparent larger diameter of the large pores, capturing the discontinuous vascular fenestrations of the organ.

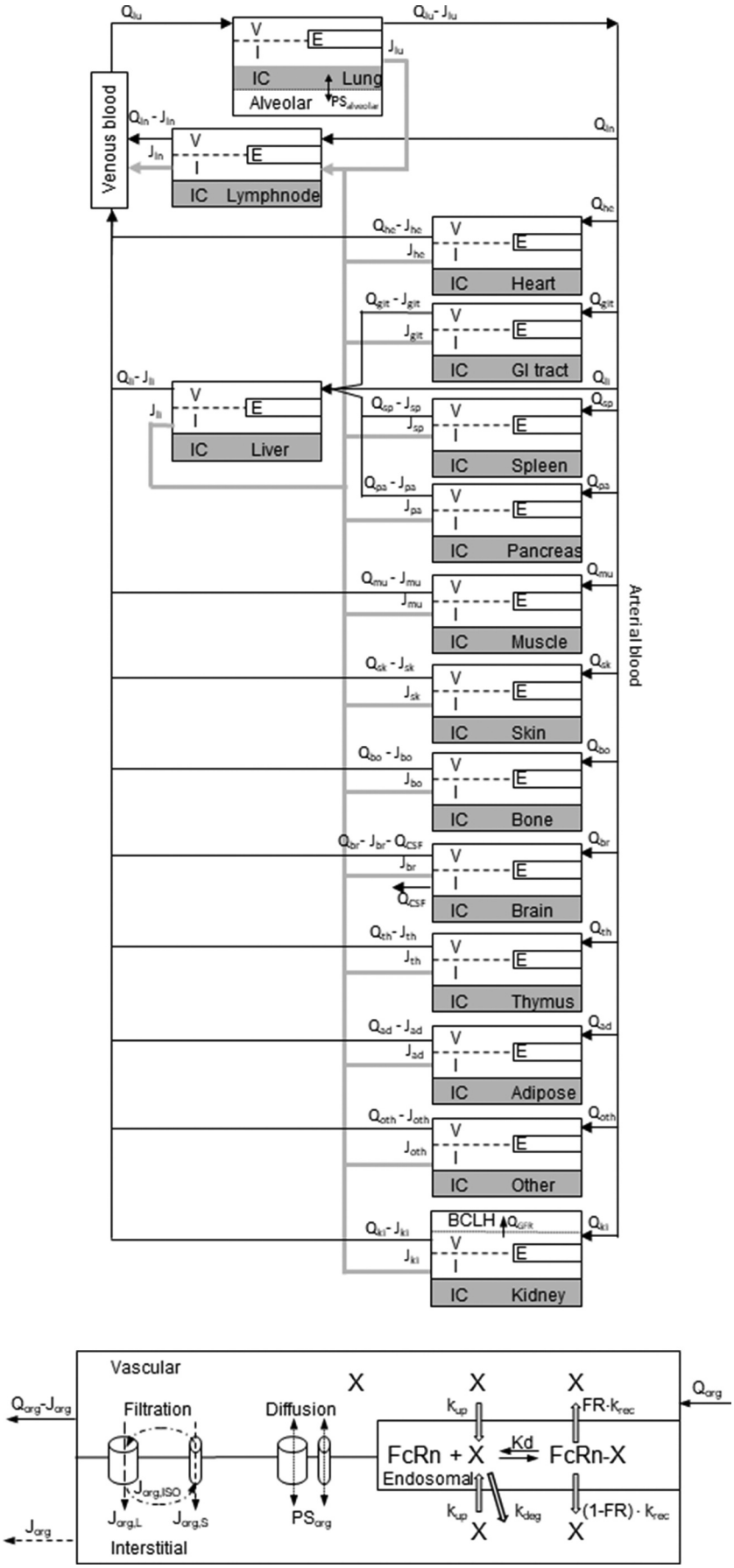

Figure 2. Structure of the whole body PBPK. (A) The organs are connected with plasma flow rate (Qorg, black line) and lymph flow rate (Jorg, gray line). Abbreviations: lung-lu, lymph nodes -ln, heart-he, GI tract-gi, liver-li, spleen-sp, pancreas-pa, skeletal muscle-mu, skin-sk, bone-bo, brain-br, thymus-th, adipose-ad, other-ot, kidney-ki. The organ subcompartments are vascular (v), interstitial (i), intracellular (IC) and endosomal (e). (B) Filtration-diffusion-driven solute exchange between the vascular and interstitial spaces takes place through small and large pores according to the two-pore hypothesis. Macropinocytosis (k_{up}) delivers extracellular proteins to the endosomal space where FcRn-mediated recycling (k_{rec}) back into vascular or interstitial space and nonspecific degradation (k_{deg}) take place. Organ-specific modifications are shown on Supplementary Figure 2.

Table 1. Parameters used for human AlbudAb-specific PBPK model.

Parameter	Unit	Value	Description	Reference
System parameters				
k_{up}	1/h	0.14	Nonspecific clearance by macropinocytosis	Equation (1)
$t_{½}$	h	80	IgG plasma half-life in humans in the absence or saturation of FcRn-mediated recycling	16–19
Vss	ml/g	0.08	Typical mAb volume of distribution in humans is around 5.5 L	20
[FcRn]	M	9.1E-6	Endosomal total FcRn based on average tissue concentration	21
[Albumin]	M	5.4E-4	Human plasma albumin concentration	16
$K_{d,albumin:FcRn}$	M	7.6E-7	Human albumin affinity for human FcRn	22
$k_{on,albumin:FcRn}$	1/(M·h)	3.2E7	Human albumin association rate constant for human FcRn	22
$k_{off,albumin:FcRn}$	1/h	24.8	Human albumin dissociation rate constant for human FcRn	22
AlbudAb parameters				
$K_{d,albumin:AlbudAb}$	M	8.5E-10	AlbudAb GSK3128349 affinity for human albumin	15
$k_{on,albumin:AlbudAb}$	1/(M·h)	3.6E9	AlbudAb GSK3128349 association rate constant	15
$k_{off,albumin:AlbudAb}$	1/h	3.1	AlbudAb GSK3128349 dissociation rate constant	15

Table 2. Fitted parameters.

Parameter	Unit	Value	%RMSE	Description
Zr_0_free	Mole	2.2E-9	(8.6)	Free ^{89}Zr or ^{89}Zr-GSK3128349 AlbudAb fragments in the dose*
Koff_Zr	1/h	9.1E-5	(10)	^{89}Zr dissociation from DFO chelate
Qurn_Zr	ml/h	0.11	(3)	Clearance of ^{89}Zr label into urine from the glomerular compartment
J_br	Dimensionless	1.1E-6	(21)	Fractional lymph flow rate in the brain
br_mp	Dimensionless	1.1E-8	(18)	Macropinocytosis rate adjustment in the brain

*computationally estimated value

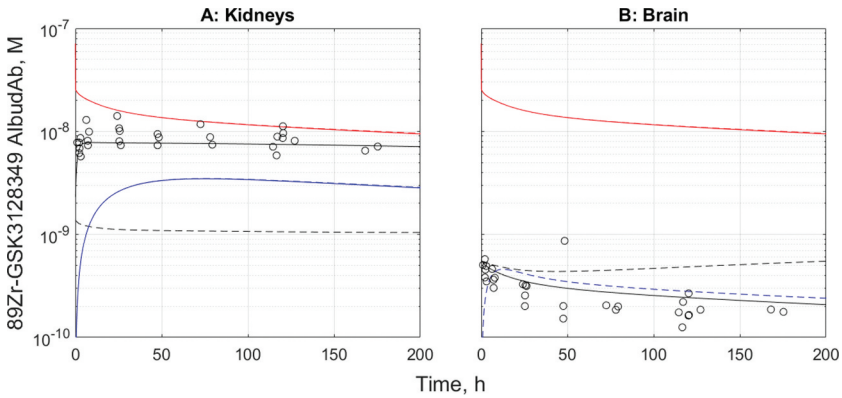

Figure 3. The tissue distribution time course results before and after fitting for kidneys (a) and the brain (b). Red: total ^{89}Zr-containing species in plasma, black-tissue average of total ^{89}Zr, blue-predicted interstitial concentration. Solid line-fitted model, dashed line-default model. Solid and dashed lines overlay for the capillary plasma compartment in both organs and for the interstitial compartment in kidneys.

In bone marrow (Figure 5(d)), the tissue concentration reaches the model-predicted steady-state level, yet the distribution phase is not well captured, with the experimental data suggesting more rapid penetration than the model predicts. This may be related to the relatively large volume of the interstitial space in bone marrow, which exceeds that of plasma vasculature some 13-fold (in liver the ratio is 3.5), but it also suggests the possibility of higher hydrodynamic conductance of bone marrow vasculature that is discontinuous in nature.

Finally, pancreas and spleen are the remaining two organs for which there is tissue distribution time course data (Figure 5(e,f)). The former has a poorly defined distribution phase, making this organ more similar to muscle rather than lungs or liver, for example. Spleen, on the other hand, is another well-perfused organ with highly permeably discontinuous vasculature, hence the tissue and plasma concentrations of ^{89}Zr-GSK3128349 AlbudAb run in parallel, although early mismatch suggests that the relative volume of the vascular compartment may be slightly underestimated in the physiological parameter set used.

In summary, the organs and tissues studied display a range of permeability, vascularization, and interstitial volumes, which result in different shapes of the tissue concentration time course curve. Steady state can be achieved rapidly or it can take longer, the interstitial concentration can almost reach the plasma levels, e.g., liver, or remain lower, especially in brain. In most of the cases the rodent-parameterized biologics PBPK model provided good to acceptable prediction for humans, while corrections were necessary to account for the residualizing label-related issues in kidneys and very slow macropinocytosis in the brain. Given that in the model macropinocytosis is assigned to the endothelial cells only, the default setup may overpredict the process in the brain where the parenchymal cells are isolated from the proteins in circulation through the tight junctions of the blood-brain-barrier (BBB).

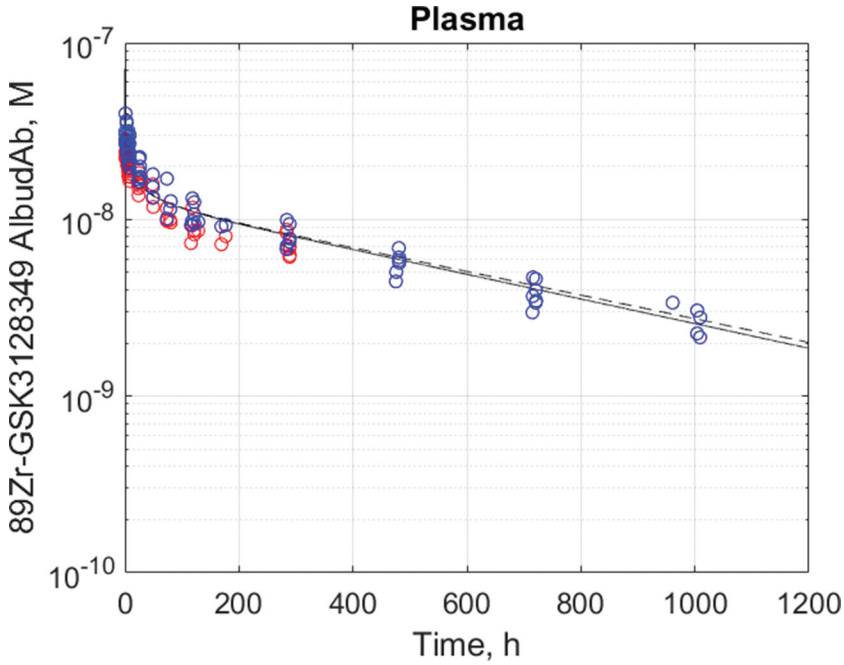

Figure 4. Plasma half-life data[14] and best fit for ^{89}Zr-GSK3128349 AlbudAb in healthy humans. AlbudAb plasma concentration: Blue: measured by mass spectrometry for AlbudAb protein, Red: measured by scintillation and PET for ^{89}Zr. Solid line-fitted model, dashed line-default model.

Discussion

A number of frameworks have been implemented to improve the clinical success rates of new drugs, including the Three Pillars at Pfizer,[11] five Rs at AstraZeneca,[30] and quality guidelines at GlaxoSmithKline.[31] All of these include focus on the drug concentration at the site of action, target engagement and downstream pharmacology. The same principles are expected to apply both to small and large molecule drugs, but the latter are primarily confined to the extracellular space, they do not diffuse across plasma membranes and extravasation occurs predominantly through protein size-dependent paracellular filtration-diffusion. In addition, the clearance of biologics can be significantly accelerated through target-mediated drug disposition (TMDD),[32] while for the small molecule drugs this is determined by the transporters and metabolizing enzymes in a target-independent fashion. In that sense, the generic biologics PBPK, e.g., the monoclonal antibody (mAb) platform model of Shah and Betts,[33] defines the 'standard' framework for a given modality in the species of choice, which needs to be further customized to account for the target-mediated and any other pharmacologically relevant interactions. The latter can involve many molecular species and reactions, resulting in large and complex models.

Model calibration for albumin

It is well known that albumin-binding activity can extend the plasma half-life of smaller protein fragments that otherwise would be rapidly eliminated through renal filtration, such as Fabs,[34] nanobodies,[35] and human domain antibodies.[36,37] At around 40 g/L, albumin is a major plasma protein, but even more, approximately 60% of the total, is estimated to be extravascular,[38] in agreement with the PBPK model-predicted fraction of 63%. Experimental data for albumin interstitial fluid concentration in specific tissues is sparse, with 200 µM and 110 µM measured in the skeletal muscle and adipose tissues by Ellmerer et al.,[39] while 2 µM has been estimated in the brain.[40] The model-predicted values for albumin interstitial concentrations for these same 3 tissues are 200 µM, 280 µM, and 0.25 µM, respectively, suggesting that whilst the overall average is in agreement with the experimental data, there can be discrepancies in both directions for individual organs. For ^{89}Zr-GSK3128349 AlbudAb, the effect of albumin concentration variation is negligible given the high affinity of the domain antibody. In most cases the free fraction is less than 0.0004%, except brain interstitium, where it may reach 0.1–1%, but even there the overall concentrations are still significantly lower than in plasma. From the mechanistic perspective it is also important to keep in mind that albumin-binding activity is included only to extend the half-life of the molecule, and it is not expected to interfere with the functional activity of any attached therapeutic payload, even when bound to albumin.

Plasma pharmacokinetics and renal filtration

The plasma PK profile and terminal half-life of ^{89}Zr-labeled and unlabeled GSK3128349 AlbudAb were found to be effectively equal to that of endogenous albumin. Due to the very low free fraction in plasma, even considerable ≈1 L/min of glomerular filtration is insufficient to significantly contribute to the overall clearance. In preclinical species, where we explicitly studied the correlation between AlbudAb affinity and plasma half-life, we found that renal elimination played a role only at dissociation constant values above 100 nM.[14] ^{89}Zr-GSK3128349 AlbudAb with subnanomolar affinity for albumin therefore effectively

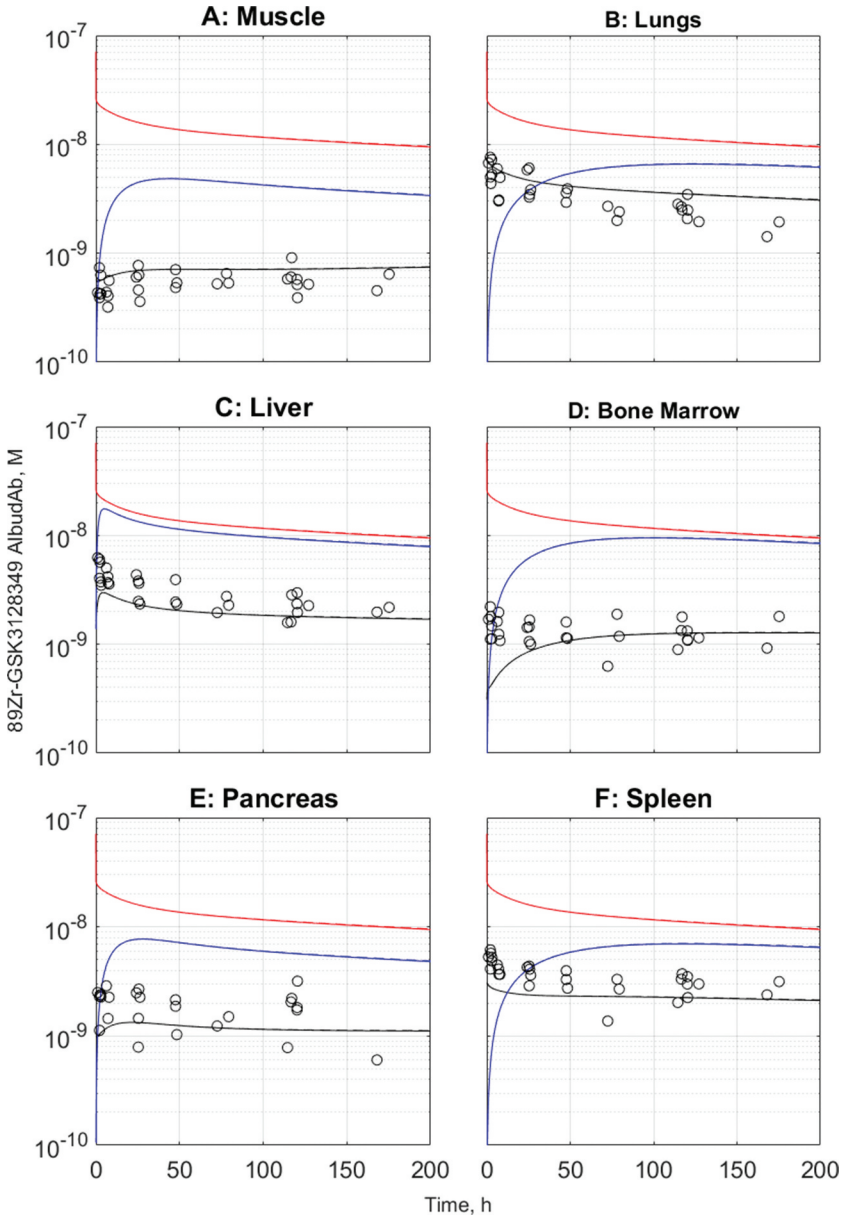

Figure 5. Observed and predicted tissue and interstitial concentrations for muscle (a), lungs (b), liver (c), bone marrow (d), pancreas (e), and spleen (f). The default model predictions are in dashed lines while the kidney- and brain-adjusted predictions are in solid lines. The solid and dashed lines overlap for all organs. Black: total tissue concentration, red: vascular concentration, blue: interstitial concentration.

functions as an irreversible label for albumin, and therefore also informs about the tissue distribution kinetics and turnover of this ubiquitous and essential carrier protein for steroids, fatty acids, thyroid hormones, and many small molecule drugs in the blood.[25]

The adjustment to the already very low glomerular sieving coefficient suggests that, whilst this parameter broadly translates from one species to another reasonably well as a function of the hydrodynamic size of the protein, there can still be species-specific differences that will only be discovered in light of experimental data. The bulk of albumin elimination though is systemic, and this depends on the rate of macropinocytosis (k_{up}) and albumin affinity for FcRn. Notably, the k_{up} value that we calculated from Equation (1) (see Materials and Methods) is around sixfold lower than for rodents[14] and suggests a slower rate of plasma protein macropinocytosis in humans. Regarding FcRn interaction with albumin, this is understood to follow 1:1 stoichometry without competition from IgG,[16] but even then there is a degree of variation in the affinity values reported in the literature, ranging from 0.4 μM to 5.2 μM,[22,41–45] of which the median at 1.1 μM was used. Three independent processes therefore affect the catabolism of albumin in the model, and the model used reconciles the reported values with the observations.

Tissue concentrations

PET/CT allows high resolution, sensitive, noninvasive and quantitative 3D high-resolution imaging and tissue concentration measurement of positron-emitting isotopes across species, including humans.[46,47] Whilst many isotopes are available, ^{89}Zr is widely used for mAbs[48] due to its relatively long 78.4-hour half-life, which can accommodate relatively slow tissue penetration of antibodies and good spatial resolution down to few

millimeters.[49] On the other hand, ^{89}Zr (like other heavy metals) is a residualizing label, unlike ^{3}H and ^{131}I, i.e., it accumulates at the site of catabolism, and the attachment to the protein of interest, albeit very stable, is noncovalent and hence potentially liable to dissociation.

Kidneys

The long plasma half-life of 430 hours indicated that ^{89}Zr-GSK3128349 AlbudAb clearance from plasma was slow and not in agreement with the rapid accumulation of approximately 2.5% of the administered dose within the first few hours after dosing. Three options were considered: incomplete albumin complex formation during dosing, the presence of noncomplexed ^{89}Zr species in the sample or inactivation of a small fraction GSK3128349 AlbudAb during the labeling process.[50] The first option was ruled out because 20000-fold molar concentration excess of vascular albumin results in about 1 ms half-life for the complex formation, i.e., this is instant for practical purposes and over by the time of first-pass renal filtration. The presence of a small amount of unconjugated ^{89}Zr-oxalate or ^{89}Zr-DFO is also unlikely because, in mice, the former has been shown to end up in bones and cartilage, while the latter, whilst renally secreted, is not retained in the kidneys.[51] Renal retention was, however, the defining feature of the ^{89}Zr signal in kidneys, with clearance from the cortical region around 500-fold slower than expected from the rate of urine formation. This therefore suggests that about 2.5% of the dosed ^{89}Zr- GSK3128349 AlbudAb, i.e., 25 μg, may have lost its albumin-binding activity either during DFO conjugation or ^{89}Zr loading steps and co-purified with the active species during the gel filtration steps aimed at removing the unbound low molecular weight reagents. The inactive ^{89}Zr-labeled GSK3128349 AlbudAb would have been rapidly eliminated through renal filtration due to its small molecular weight of 13 kDa, absorbed in proximal tubules through nonspecific megalin-cubilin-mediated uptake and then catabolized into amino acids,[52–54] with ^{89}Zr-DFO-Lys degradation product retained in the cells.

The fitted model provided a rate constant corresponding to a 700-hour half-life with relatively low error margin for the production of ^{89}Zr-labeled species that are subject to renal filtration. This process can correspond to the dissociation of ^{89}Zr from the chelate or inactivation of the AlbudAb (or their combination). Zr equilibrium with DFO is strongly shifted toward the complex, but remains rapidly reversible as demonstrated by the dissociating effect of excess free competing chelator, e.g., ethylenediaminetetraacetic acid.[55] Likewise, around 0.2% of ^{89}Zr was found to have dissociated during 24-hour incubation in plasma in vitro,[56] which would be subject to renal filtration with possibility of accumulating to PET-detectable levels in the small volume of kidneys. Given the patterns of ^{89}Zr tissue distribution dependence on the compound, be it chloride, oxalate or DFO chelate,[51] this is an aspect that needs to be considered whilst interpreting the tissue distribution data of ^{89}Zr-labeled proteins in immunoPET studies.

Brain

Low brain levels of ^{89}Zr-GSK3128349 AlbudAb found in the current study, where the entire signal was attributable to the AlbudAb in brain vasculature, aligns well with the observation by Bensch et al.[57] of very low uptake of ^{89}Zr-labeled mAbs. At the expected 200-fold or even higher dilution between brain interstitial and vascular spaces, the PET signal from interstitial space would have made up no more than 2.5% of the total, i.e., its contribution remained below the accuracy of the experiment. Likewise, the plasma and organ concentrations remained parallel in the time course plot for the brain, suggesting no significant irreversible accumulation either, through macropinocytosis and endosomal degradation. This was formally captured through brain macropinocytosis adjustment coefficient br_mp being effectively zero in the best fit model, which excluded the possibility of ^{89}Zr accumulation and contribution to the observed signal. The fractional brain lymph flow estimate from the human data set is therefore lower than that from the rodent data.[14] Whilst this can be species-specific variation, i.e., rodent BBB may be more permeable, it is noteworthy that the brain concentrations measured in mouse brains by quantitative whole-body autoradiography imaging were consistently lower than those measured in rats by quantitative radiochemical analysis where small tissue samples are excised, incinerated and the released radioactivity counted. In addition, what makes the brain interstitium especially challenging, is not only the tightness of BBB, but also relatively rapid turnover of the interstitial fluid in the central nervous system, where this happens once every 10 hours due to vigorous influx of water via dedicated aquaporin channels.[58] This very simplified presentation of brain in our model is shown on Supplementary Figure 2A, whilst more detailed implementation has been introduced by Chang et al.[59]

Other tissues

The kidneys and brain were examples of two organs that were modified beyond the default layout to capture their respective specifics. In addition, the lung is also modified automatically with the alveolar epithelial lining fluid layer added and connected to the interstitium, but minor amounts of centrally dosed biologics reach there to make a difference to the overall tissue concentration. It can be concluded therefore that the default organ layout allowed good to satisfactory prediction of the human tissue distribution properties of ^{89}Zr-GSK3128349 AlbudAb. In all cases the steady state levels of total tissue concentrations were correctly predicted and, in most cases, also the distribution phase tissue penetration kinetics. The latter is remarkable given that the vascular capillaries in spleen, lymph nodes and liver are of the discontinuous sinusoidal type where the paracellular gaps can be large enough to allow the passage of cells and the two-pore approach of Rippe and Haraldsson[12] becomes less applicable. Therefore, the literature-sourced parameters used in our preclinical paper[14] captured well the distribution phase even in organs with discontinuous capillaries, except in the case of bone marrow, where the experimental data indicate rapid reaching of the steady state while the model predicted a slower process. Interestingly, similar rapid bone marrow extravasation kinetics was also observed in mice and rats, suggesting that the interstitial volume parameter may be too high and/or the fractional lymph flow too low.

Biologics PBPK in drug discovery process

AlbudAb PBPK model describes the concentration time courses for the free and albumin-bound species of GSK3128349 in different tissue compartments, but it would need to be expanded and adapted if other modalities or interactions were to be included. The latter aspect is uniquely important for biologics because, unlike small molecule drugs, their tissue distribution and elimination can be drastically affected by target-mediated processes which are not included in the model described.

For example, in the case of ibalizumab, a CD4-binding mAb approved for the treatment of AIDS,[60] the target-bound antibody is rapidly internalized and degraded, resulting in only five-day half-life of the drug in humans. By adapting the biologics PBPK model to ibalizumab and CD4, as outlined on Supplementary Figure 4, we captured this aspect of ibalizumab PK by quantifying the internalization rate constant value for CD4-ibalizumab complex and identified another hitherto unappreciated aspect of CD4 targeting, limited exposure to the drug in organs with high local levels of $CD4^+$ T cells, as shown on Figure 6. The effect is less pronounced for lymph nodes, which are on the main pathway of lymphatic circulation, but in spleen the free ibalizumab concentration can be around 400-fold lower than in plasma due to TMDD. As a result, relatively high antibody concentration in plasma needs to be maintained to achieve acceptable exposure in spleen. This is indeed the situation at the recommended dosing regimen where antibody trough plasma concentration of 200 nM, whilst sufficient for >99.98% target engagement at Kd = 83 pM[61] (and >2000-fold excess over $IC_{50} \approx 100$ pM potency[62]) in blood, provides only two to threefold excess in the spleen to contain the infectivity of HIV.[63]

From the methodological point of view it is occasionally pointed out that relatively large number of parameters are used in PBPK compared with one- or two-compartment approaches.[64] Whilst the high parameter number is true for two-pore biologics PBPK, the vast majority of them, from universal gas constant R and Avogadro number to physiological parameters like organ volumes and plasma flow rates are invariant and independent of the model, i.e., they are latent. The second group of such latent parameters are those that are indirectly estimated from experimental data and are to an extent model-dependent, e.g., organ-specific lymph flows, but these too are not varied from one model to another. Finally, there are parameters that are fitted within a specific implementation of the model, for example to capture the rate of TMDD, but which also depend on other assumptions or estimates, e.g., receptor numbers, cell numbers, tissue distribution. Only one parameter, the internalization rate constant for ibalizumab-CD4 complex, had to be estimated for the ibalizumab PBPK model described above, for example. In that sense, PBPK may provide a more frugal framework for handling complex situations than more simple ones.

In summary, we have demonstrated that the biologics PBPK framework we established using a series of inert tracer proteins in rodents[13,14] provided good to satisfactory extrapolation to humans without significant further parameterization. The resulting framework can be extended and adapted to more complex and clinically relevant scenarios for informative insight, as described for ibalizumab. Finally, all this is only possible with computer-assisted model building, which removes the major bottleneck of large complex model assembly.[14]

Materials and methods

AlbudAb PBPK model

The model describes GSK3128349 AlbudAb with and without ^{89}Zr, as well as their respective complexes with endogenous albumin, as outlined on Figure 1. It includes lungs,

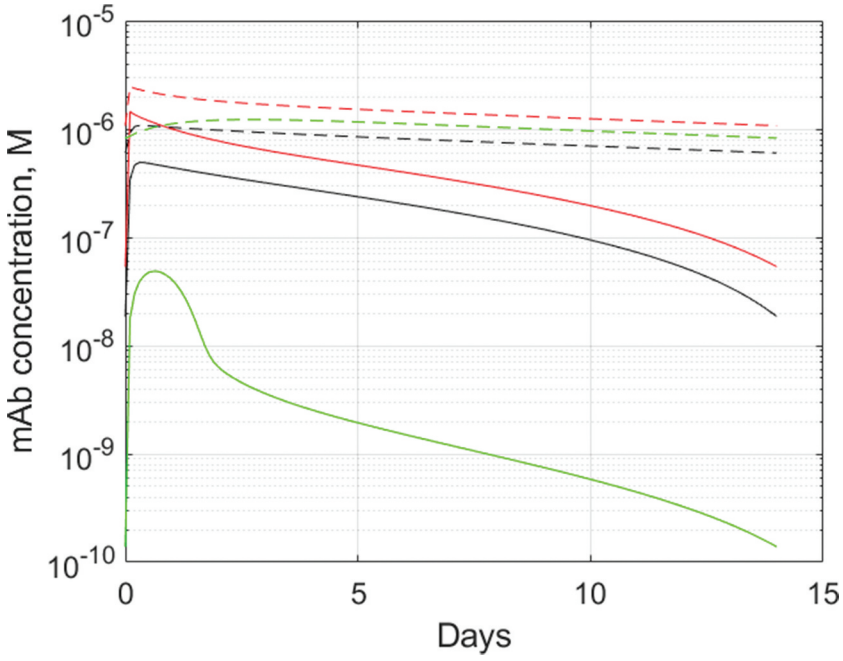

Figure 6. Predicted plasma and tissue interstitial concentrations of ibalizumab during a steady state 800 mg Q2W dosing. Solid lines: ibalizumab, dashed lines: hypothetical isotope control mAb with 20-day half-life and linear pharmacokinetics. Red: plasma, black: lymph node interstitium, green: spleen interstitium. The PBPK model used and parameterization is described in Supplementary Section.

lumped lymph nodes, heart, lumped gastrointestinal tract, liver, spleen, pancreas, muscle, skin, bone, brain, thymus, adipose tissue, and kidney, as shown on Figure 2(a). These organs account for about 98% of the body and the balance is represented by 'other' to account for the total body volume and blood flow rate. Peripheral blood is represented as a venous plasma compartment, while all organs contain vascular, interstitial, and endosomal compartments where all the relevant chemical and flow reactions take place (Figure 2(b)). All molecules are subject to two-pore filtration-diffusion exchange[14] between vascular and interstitial spaces, as outlined in detail on Supplementary Figure 2. Plasma albumin concentration was fixed at the physiological value of 540 μM in central and all organ vascular compartments, while those in the interstitial and endosomal compartments were at model-defined steady-state values.

Endosomal uptake is modeled as nonspecific macropinocytosis from vascular and interstitial spaces into endosomal compartment where the FcRn, with no decay or turnover of its own, interacts with albumin and AlbudAb-albumin complexes. Free endosomal molecular species not bound to FcRn are subject to nonspecific degradation, while the bound ones are recycled and released into interstitial and vascular spaces. Any free ^{89}Zr taken up from extracellular space, or released during the endosomal degradation process, is retained in the respective organ endosomal space to account for the residualizing nature of that radio-isotope. The free ^{89}Zr species also accounts for the ^{89}Zr-AlbudAb that may have lost the albumin-binding activity before or during the dosing event, as from the kinetic point of view these species are indistinguishable in the experimental data available (Supplementary Information).

The final PBPK model used for AlbudAb is given in Supplementary Information (AlbudAb_PBPK.sbproj).

PBPK model parameters

Physiological parameters

We are using the physiological parameters described in our previous paper[14] with the values tabulated in the Supplementary File AlbudAb.xlsx. The organ vascular plasma and interstitial space volumes are from Shah and Betts,[33] which are largely based on those of Graf et al.[65] Peripheral plasma volume was defined as the difference between the total plasma volume and the sum of organ vascular volumes. Only half of the interstitial volumes was defined as accessible given that albumin and antibodies only reach 50% of the interstitial space available, as described by Wiig et al.[66]

FcRn was assigned to the endosomal compartment, the volume of which was fixed at 0.5% of that of total tissue as previously reported.[33,67,68] Total FcRn concentration in the endosomal compartment was set at 9 μM, the weighted average scaled from the mass spectrometry measured total tissue concentrations by Fan et al[21] and found to be optimal in biologics PBPK.[14]

Nonspecific uptake of proteins from extracellular space into the endosomal compartment by macropinocytosis was characterized by clearance parameter k_{up}, calculated according Equation (1), as introduced in Sepp et al.[14]

$$k_{up} = \frac{0.693 \cdot V_{ss} \cdot d}{0.005 \cdot t_{1/2}} \quad (1)$$

where d is the tissue density (assumed to be 1 g/ml), Vss (ml/kg) is the typical volume of distribution of large proteins like albumin and IgG in humans and $t_{½}$ is the IgG half-life in humans in the absence or saturation of FcRn-mediated recycling; a proxy for nonspecific default degradation of all proteins not subject to specific degradation or renal elimination. The equation gives the specific average clearance of soluble proteins from extracellular space via macropinocytosis. It was assumed that k_{up} was the same for all protein species.

Software

Matlab R2019a and SimBiology™ version 5.8.2 were used to build the PBPK model and perform data analysis. Matlab script PBPKassembler.m (Supplementary Information) developed by us previously[14] was used to build the SimBiology-compliant full biologics PBPK model from the molecular species and reactions outlined in GenericTissue and thereafter manually adjusted as described in Supplementary section.

PET measures the average concentration across all tissue subcompartments and the signal does not depend on the nature of the molecular species that the label is attached to. As a result, the organ concentrations of ^{89}Zr used in curve fitting were calculated by summing up the molar amounts of all ^{89}Zr-containing molecular species in the given organ vascular, interstitial, and endosomal compartments and then dividing this with the organ volume.

Abbreviations

BBB	Blood-brain-barrier
DFO	Desferrioxamine
FcRn	Neonatal Fc receptor
immunoPET	Immuno-positron emission tomography
mAb	Monoclonal antibody
PBPK	Physiologically based pharmacokinetics
PET	Positron emission tomography
PET/CT	Positron emission tomography-computed tomography
PK	Pharmacokinetics
TMDD	Target-mediated drug disposition

Disclosure of Potential Conflicts of Interest

All authors are employees of GlaxoSmithKline Plc.

References

1. Carter PJ, Lazar GA. Next generation antibody drugs: pursuit of the 'high-hanging fruit'. Nat Rev Drug Discov. 2017;17:197–223.
2. Lagassé HAD, Alexaki A, Simhadri VL, Katagiri NH, Jankowski W, Sauna ZE, Kimchi-Sarfaty C. Recent advances in (therapeutic protein) drug development. F1000Res. 2017;6:113. doi:10.12688/f1000research.9970.1.
3. Ward ES, Gussow D, Griffiths AD, Jones PT, Winter G. Binding activities of a repertoire of single immunoglobulin variable domains secreted from Escherichia coli. Nature. 1989;341:544–46. doi:10.1038/341544a0.
4. Jespers L, Schon O, Famm K, Winter G. Aggregation-resistant domain antibodies selected on phage by heat denaturation. Nat Biotechnol. 2004;22:1161–65. doi:10.1038/nbt1000.

5. Sheridan C. Ablynx's nanobody fragments go places antibodies cannot. Nat Biotechnol. 2017;35:1115. doi:10.1038/nbt1217-1115.
6. Ellerman D. Bispecific T-cell engagers: towards understanding variables influencing the in vitro potency and tumor selectivity and their modulation to enhance their efficacy and safety. Methods. 2019;154:102–17. doi:10.1016/j.ymeth.2018.10.026.
7. Wensel D, Sun Y, Li Z, Zhang S, Picarillo C, McDonagh T, Fabrizio D, Cockett M, Krystal M, Davis J, et al. Discovery and characterization of a novel CD4-binding adnectin with potent anti-HIV activity. Antimicrob Agents Chemother. 2017;61: e00508–17. doi:10.1128/AAC.00508-17.
8. Plückthun A. Designed Ankyrin Repeat Proteins (DARPins): binding proteins for research, diagnostics, and therapy. Annu Rev Pharmacol Toxicol. 2015;55:489–511. doi:10.1146/annurev-pharmtox-010611-134654.
9. Rothe C, Skerra A. Anticalin(®) proteins as therapeutic agents in human diseases. BioDrugs. 2018;32:233–43. doi:10.1007/s40259-018-0278-1.
10. Boudousquie C, Bossi G, Hurst JM, Rygiel KA, Jakobsen BK, Hassan NJ. Polyfunctional response by ImmTAC (IMCgp100) redirected CD8(+) and CD4(+) T cells. Immunology. 2017;152:425–38. doi:10.1111/imm.12779.
11. Morgan P, Van Der Graaf PH, Arrowsmith J, Feltner DE, Drummond KS, Wegner CD, Street SDA. Can the flow of medicines be improved? Fundamental pharmacokinetic and pharmacological principles toward improving phase II survival. Drug Discov Today. 2012;17:419–24.
12. Rippe B, Haraldsson B. Transport of macromolecules across microvascular walls: the two-pore theory. Physiol Rev. 1994;74:163–219. doi:10.1152/physrev.1994.74.1.163.
13. Sepp A, Berges A, Sanderson A, Meno-Tetang G. Development of a physiologically based pharmacokinetic model for a domain antibody in mice using the two-pore theory. J Pharmacokinet Pharmacodyn. 2015;42:97–109. doi:10.1007/s10928-014-9402-0.
14. Sepp A, Meno-Tetang G, Weber A, Sanderson A, Schon O, Berges A. Computer-assembled cross-species/cross-modalities two-pore physiologically based pharmacokinetic model for biologics in mice and rats. J Pharmacokinet Pharmacodyn. 2019;46:339–59. doi:10.1007/s10928-019-09640-9.
15. Thorneloe KS, Sepp A, Zhang S, Galinanes-Garcia L, Galette P, Al-Azzam W, Vugts DJ, van Dongen G, Elsinga P, Wiegers J, et al. The biodistribution and clearance of AlbudAb, a novel biopharmaceutical medicine platform, assessed via PET imaging in humans. EJNMMI Res. 2019;9:45. doi:10.1186/s13550-019-0514-9.
16. Kim J, Hayton WL, Robinson JM, Anderson CL. Kinetics of FcRn-mediated recycling of IgG and albumin in human: pathophysiology and therapeutic implications using a simplified mechanism-based model. Clin Immunol. 2007;122:146–55. doi:10.1016/j.clim.2006.09.001.
17. Waldmann TA, Strober W. Metabolism of immunoglobulins. Prog Allergy. 1969;13:1–110.
18. Waldmann TA, Terry WD. Familial hypercatabolic hypoproteinemia. A disorder of endogenous catabolism of albumin and immunoglobulin. J Clin Invest. 1990;86:2093–98. doi:10.1172/JCI114947.
19. Wani MA, Haynes LD, Kim J, Bronson CL, Chaudhury C, Mohanty S, Waldmann TA, Robinson JM, Anderson CL. Familial hypercatabolic hypoproteinemia caused by deficiency of the neonatal Fc receptor, FcRn, due to a mutant β2-microglobulin gene. Proc Natl Acad Sci USA. 2006;103:5084–89. doi:10.1073/pnas.0600548103.
20. Lobo ED, Hansen RJ, Balthasar JP. Antibody pharmacokinetics and pharmacodynamics. J Pharm Sci. 2004;93:2645–68. doi:10.1002/jps.20178.
21. Fan -Y-Y, Avery LB, Wang M, O'Hara DM, Leung S, Neubert H. Tissue expression profile of human neonatal Fc receptor (FcRn) in Tg32 transgenic mice. mAbs. 2016;8:848–53. doi:10.1080/19420862.2016.1178436.
22. Cameron J, Sleep D, Sandlie I, Andersen JT Pharmacokinetic animal model. WO 2014/125082, Google Patents; 2014.
23. Beeken WL, Volwiler W, Goldsworthy PD, Garby LE, Reynolds WE, Stogsdill R, Stemler RS. Studies of I-131-albumin catabolism and distribution in normal young male adults. J Clin Invest. 1962;41:1312–33. doi:10.1172/JCI104594.
24. Anderson CL, Chaudhury C, Kim J, Bronson CL, Wani MA, Mohanty S. Perspective – fcRn transports albumin: relevance to immunology and medicine. Trends Immunol. 2006;27:343–48. doi:10.1016/j.it.2006.05.004.
25. Levitt DG, Levitt MD. Human serum albumin homeostasis: a new look at the roles of synthesis, catabolism, renal and gastrointestinal excretion, and the clinical value of serum albumin measurements. Int J Gen Med. 2016;9:229–55. doi:10.2147/IJGM.S102819.
26. Vincent J-L, Russell JA, Jacob M, Martin G, Guidet B, Wernerman J, Roca R, McCluskey SA, Gattinoni L. Albumin administration in the acutely ill: what is new and where next? Crit Care. 2014;18:231. doi:10.1186/cc13991.
27. Tojo A, Kinugasa S. Mechanisms of glomerular albumin filtration and tubular reabsorption. Int J Nephrol. 2012;2012:9. doi:10.1155/2012/481520.
28. Norden AGW, Lapsley M, Lee PJ, Pusey CD, Scheinman SJ, Tam FWK, Thakker RV, Unwin RJ, Wrong O. Glomerular protein sieving and implications for renal failure in Fanconi syndrome. Kidney Int. 2001;60:1885–92. doi:10.1046/j.1523-1755.2001.00016.x.
29. Rutili G, Arfors K-E. Protein concentration in interstitial and lymphatic fluids from the subcutaneous tissue. Acta Physiol Scand. 1977;99:1–8. doi:10.1111/j.1748-1716.1977.tb10345.x.
30. Morgan P, Brown DG, Lennard S, Anderton MJ, Barrett JC, Eriksson U, Fidock M, Hamrén B, Johnson A, March RE, et al. Impact of a five-dimensional framework on R&D productivity at AstraZeneca. Nat Rev Drug Discov. 2018;17:167–181.
31. Bayliss MK, Butler J, Feldman PL, Green DVS, Leeson PD, Palovich MR, Taylor AJ. Quality guidelines for oral drug candidates: dose, solubility and lipophilicity. Drug Discov Today. 2016;21:1719–27. doi:10.1016/j.drudis.2016.07.007.
32. Petitcollin A, Bensalem A, Verdier M-C, Tron C, Lemaitre F, Paintaud G, Bellissant E, Ternant D. Modelling of the time-varying pharmacokinetics of therapeutic monoclonal antibodies: a literature review. Clin Pharmacokinet. 2020;59:37–49. doi:10.1007/s40262-019-00816-7.
33. Shah DK, Betts AM. Towards a platform PBPK model to characterize the plasma and tissue disposition of monoclonal antibodies in preclinical species and human. J Pharmacokinet Pharmacodyn. 2012;39:67–86. doi:10.1007/s10928-011-9232-2.
34. Nguyen A, Reyes AE, Zhang M, McDonald P, Wong WLT, Damico LA, Dennis MS. The pharmacokinetics of an albumin-binding Fab (AB.Fab) can be modulated as a function of affinity for albumin. Protein Eng Des Sel. 2006;19:291–97. doi:10.1093/protein/gzl011.
35. Hoefman S, Ottevaere I, Baumeister J, Sargentini-Maier ML. Preclinical intravenous serum pharmacokinetics of albumin binding and non-half-life extended nanobodies®. Antibodies. 2015;4:141–56. doi:10.3390/antib4030141.
36. Holt LJ, Basran A, Jones K, Chorlton J, Jespers LS, Brewis ND, Tomlinson IM. Anti-serum albumin domain antibodies for extending the half-lives of short lived drugs. Protein Eng Des Sel. 2008;21:283–88. doi:10.1093/protein/gzm067.
37. Herring C, Schon O. AlbudAb™ technology platform–versatile albumin binding domains for the development of therapeutics with tunable half-lives. Therapeutic Proteins: Wiley-VCH Verlag GmbH & Co. KGaA; 2012. p. 249–68.
38. Rothschild MA, Bauman A, Yalow RS, Berson SA. Tissue distribution of I131 labeled human serum albumin following intravenous administration. J Clin Invest. 1955;34:1354–58. doi:10.1172/JCI103183.
39. Ellmerer M, Schaupp L, Brunner GA, Sendlhofer G, Wutte A, Wach P, Pieber TR. Measurement of interstitial albumin in human skeletal muscle and adipose tissue by open-flow microperfusion. Am J Physiol Endocrinol Metab. 2000;278:E352–E6. doi:10.1152/ajpendo.2000.278.2.E352.

40. Hladky SB, Barrand MA. Mechanisms of fluid movement into, through and out of the brain: evaluation of the evidence. Fluids Barriers CNS. 2014;11:26. doi:10.1186/2045-8118-11-26.
41. Andersen JT, Daba MB, Berntzen G, Michaelsen TE, Sandlie I. Cross-species binding analyses of mouse and human neonatal fc receptor show dramatic differences in immunoglobulin G and albumin binding. J Biol Chem. 2010;285:4826–36. doi:10.1074/jbc.M109.081828.
42. Andersen JT, Cameron J, Plumridge A, Evans L, Sleep D, Sandlie I. Single-chain variable fragment albumin fusions bind the neonatal Fc receptor (FcRn) in a species dependent manner: implications for in vivo half-life evaluation of albumin-fusion therapeutics. J Biol Chem. 2013;288:24277–85. doi:10.1074/jbc.M113.463000.
43. Andersen JT, Dalhus B, Viuff D, Thue Ravn B, Gunnarsen KS, Plumridge A, Bunting K, Antunes F, Williamson R, Athwal S, et al. Extending serum half-life of albumin by engineering FcRn binding. J Biol Chem. 2014;289:13492–502. doi:10.1074/jbc.M114.549832.
44. Viuff D, Antunes F, Evans L, Cameron J, Dyrnesli H, Thue Ravn B, Stougaard M, Thiam K, Andersen B, Kjærulff S, et al. Generation of a double transgenic humanized neonatal Fc receptor (FcRn)/albumin mouse to study the pharmacokinetics of albumin-linked drugs. J Controlled Release. 2016;223:22–30. doi:10.1016/j.jconrel.2015.12.019.
45. Nilsen J, Bern M, Sand KMK, Grevys A, Dalhus B, Sandlie I, Andersen JT. Human and mouse albumin bind their respective neonatal Fc receptors differently. Sci Rep. 2018;8:14648. doi:10.1038/s41598-018-32817-0.
46. Gambhir SS. Molecular imaging of cancer with positron emission tomography. Nat Rev Cancer. 2002;2:683. doi:10.1038/nrc882.
47. Lamberts LE, Williams SP, Terwisscha van Scheltinga AGT, Lub-de Hooge MN, Schröder CP, Gietema JA, Brouwers AH, de Vries EGE. Antibody positron emission tomography imaging in anticancer drug development. J Clin Oncol. 2015;33:1491–504. doi:10.1200/JCO.2014.57.8278.
48. van Dongen GAMS, Vosjan MJWD. Immuno-positron emission tomography: shedding light on clinical antibody therapy. Cancer Biother Radiopharm. 2010;25:375–85. doi:10.1089/cbr.2010.0812.
49. Deri MA, Zeglis BM, Francesconi LC, Lewis JS. PET imaging with ^{89}Zr: from radiochemistry to the clinic. Nucl Med Biol. 2013;40:3–14. doi:10.1016/j.nucmedbio.2012.08.004.
50. Vosjan MJWD, Perk LR, Visser GWM, Budde M, Jurek P, Kiefer GE, van Dongen GAMS. Conjugation and radiolabeling of monoclonal antibodies with zirconium-89 for PET imaging using the bifunctional chelate p-isothiocyanatobenzyl-desferrioxamine. Nat Protoc. 2010;5:739. doi:10.1038/nprot.2010.13.
51. Holland JP, Divilov V, Bander NH, Smith-Jones PM, Larson SM, Lewis JS. 89Zr-DFO-J591 for immunopet of prostate-specific membrane antigen expression in vivo. J Nucl Med. 2010;51:1293–300. doi:10.2967/jnumed.110.076174.
52. Haraldsson B, Nystrom J, Deen WM. Properties of the glomerular barrier and mechanisms of proteinuria. Physiol Rev. 2008;88:451–87. doi:10.1152/physrev.00055.2006.
53. Haraldsson B, Jeansson M. Glomerular filtration barrier. Curr Opin Nephrol Hypertens. 2009;18:331–35. doi:10.1097/MNH.0b013e32832c9dba.
54. Comper WD, Deen WM, Haraldsson B. Resolved: normal glomeruli filter nephrotic levels of albumin. J Am Soc Nephrol. 2008;19:427–32. doi:10.1681/ASN.2007090997.
55. Raavé R, Sandker G, Adumeau P, Jacobsen CB, Mangin F, Meyer M, Moreau M, Bernhard C, Da Costa L, Dubois A, et al. Direct comparison of the in vitro and in vivo stability of DFO, DFO* and DFOcyclo* for 89Zr-immunoPET. Eur J Nucl Med Mol Imaging. 2019;46:1966–77. doi:10.1007/s00259-019-04343-2.
56. Meijs WE, Herscheid JDM, Haisma HJ, Pinedo HM. Evaluation of desferal as a bifunctional chelating agent for labeling antibodies with Zr-89. Int J Rad Appl Instrum A. 1992;43:1443–47. doi:10.1016/0883-2889(92)90170-J.
57. Bensch F, Smeenk MM, van Es SC, de Jong JR, Schröder CP, Oosting SF, Lub-de Hooge MN, Menke-van der Houven van Oordt CW, Brouwers AH, Boellaard R, et al. Comparative biodistribution analysis across four different ^{89}Zr-monoclonal antibody tracers-the first step towards an imaging warehouse. Theranostics. 2018;8:4295–304. doi:10.7150/thno.26370.
58. Nakada T, Kwee IL. Fluid dynamics inside the brain barrier: current concept of interstitial flow, glymphatic flow, and cerebrospinal fluid circulation in the brain. Neuroscientist. 2018;25:155–66. doi:10.1177/1073858418775027.
59. Chang H-Y, Wu S, Meno-Tetang G, Shah DK. A translational platform PBPK model for antibody disposition in the brain. J Pharmacokinet Pharmacodyn. 2019;46:319–38. doi:10.1007/s10928-019-09641-8.
60. Iacob SA, Iacob DG. Ibalizumab targeting CD4 receptors, an emerging molecule in HIV therapy. Front Microbiol. 2017;8:2323. doi:10.3389/fmicb.2017.02323.
61. Song R, Franco D, Kao C-Y, Yu F, Huang Y, Ho DD. Epitope mapping of ibalizumab, a humanized anti-CD4 monoclonal antibody with anti-HIV-1 activity in infected patients. J Virol. 2010;84:6935–42. doi:10.1128/JVI.00453-10.
62. Jacobson JM, Kuritzkes DR, Godofsky E, DeJesus E, Larson JA, Weinheimer SP, Lewis ST. Safety, pharmacokinetics, and antiretroviral activity of multiple doses of ibalizumab (formerly TNX-355), an anti-CD4 monoclonal antibody, in human immunodeficiency virus type 1-infected adults. Antimicrob Agents Chemother. 2009;53:450–57. doi:10.1128/AAC.00942-08.
63. Wong JK, Yukl SA. Tissue reservoirs of HIV. Curr Opin HIV AIDS. 2016;11:362–70. doi:10.1097/COH.0000000000000293.
64. Ganusov VV. Strong inference in mathematical modeling: a method for robust science in the twenty-first century. Front Microbiol. 2016;7. doi:10.3389/fmicb.2016.01131.
65. Graf JF, Scholz BJ, Zavodszky MI. BioDMET: a physiologically based pharmacokinetic simulation tool for assessing proposed solutions to complex biological problems. J Pharmacokinet Pharmacodyn. 2012;39:37–54. doi:10.1007/s10928-011-9229-x.
66. Wiig H, Gyenge C, Iversen PO, Gullberg D, Tenstad O. The role of the extracellular matrix in tissue distribution of macromolecules in normal and pathological tissues: potential therapeutic consequences. Microcirculation. 2008;15:283–96. doi:10.1080/10739680701671105.
67. Garg A, Balthasar J. Physiologically-based pharmacokinetic (PBPK) model to predict IgG tissue kinetics in wild-type and FcRn-knockout mice. J Pharmacokinet Pharmacodyn. 2007;34:687–709. doi:10.1007/s10928-007-9065-1.
68. Hansen RJ, Balthasar JP. Pharmacokinetic/pharmacodynamic modeling of the effects of intravenous immunoglobulin on the disposition of antiplatelet antibodies in a rat model of immune thrombocytopenia. J Pharm Sci. 2003;92:1206–15. doi:10.1002/jps.10364.